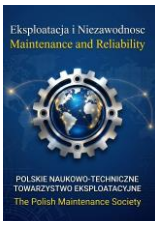

Eksploatacja i Niezawodnosc - Maintenance and Reliability

Volume 29 (2027), Issue 1

https://ein.org.pl

The Polish Maintenance Society

The local load-carrying capacity of composite structures undergoing bending under variable boundary conditions

Patryk Różyło[1,*], Paweł Wysmulski[1]

[1] Politechnika Lubelska, Poland
* Corresponding Author: p.rozylo@pollub.pl

Received: 2 April 2026
Revised: 22 May 2026
Accepted: 25 June 2026
Online: 17 July 2026

Abstract

The research focused on thin-walled composite columns made of carbon fiber reinforced polymer (CFRP). The test specimens were thin-walled, rectangular composite columns. The test specimens had identical geometric parameters and material properties. The research involved static three-point bending tests and used universal testing machine and non-destructive methods to evaluate the behaviour of the structure. The paper primarily focused on evaluating the load-carrying capacity of the structure and identifying the stages of composite material damage. The study analysed two main aspects: the effect of support spacing and specimen positioning relative to the supports on the structure's behaviour, particularly in terms of damage. Both of these aspects are presented separately in the paper, with the impact of each demonstrated in the results. Considering the positioning method of specimens relative to the supports, the specimens exhibited an average load-carrying capacity that was 1.13 times higher when the load was applied to the narrower surfaces of the specimens than to the wider surfaces. In addition, it was found that the specimens demonstrated the highest maximum load when the support spacing was smallest (100 mm). For samples where the load was applied over a wider surface area, the load was 1.21 times higher for a support spacing of 100 mm than for 150 mm. A similar situation occurred for samples where the load was applied over a narrower surface, with a ratio of 1.15 for an analogous support spacing.

Keywords: *composite columns, damage, three-point bending, non-destructive methods*

Article citation:
Różyło P, Wysmulski P, The local load-carrying capacity of composite structures undergoing bending under variable boundary conditions, Eksploatacja i Niezawodnosc – Maintenance and Reliability 2027: 29(1) http://doi.org/10.17531/ein/225077

Highlights

- NDT methods were used to assess the damage to composite.
- The effect of different support spacings during bending on composite damage was studied.
- The effect of varying samples' positions relative to the supports under bending was tested.

1. Introduction

The load-carrying capacity of thin-walled composite structures is a popular research topic among scientists [1–3]. Broad areas of research into load-carrying capacity primarily concern static strength tests based on traditional static tests, such as compression or bending. Most tests in this field include compression-based tests [4–6]. Consequently, the behaviour of the structure is typically analysed in a buckling state (buckling analysis) and post-buckling state [4–6], where composite material failure is examined in greater detail [7–10]. In tests involving bending, the focus was on the load-carrying capacity of the structure and the analysis of damage resulting from bending. Due to the complex nature of composite material damage, it is important to use independent research techniques to capture the phenomenon of failure in both quantitative and qualitative contexts. Although many research methods are available for assessing composite material damage, several well-known, commonly used methods are employed, most of which are non-destructive testing methods [11–14]. In addition to the traditional use of a universal testing machine for bending tests (usually three-point bending) [15–16], non-destructive methods are employed to assess the behaviour of structures, enabling the recording of the damage phenomenon from initiation to detection of the composite material's complex failure mechanism [17–20]. A commonly used device for non-destructive testing is an acoustic signal-recording system, also known as the acoustic emission method [21]. Acoustic emission-based tests usually make it possible to identify composite material damage and assess the stage of damage initiation and further evolution by analysing the intensity of registered acoustic signals. The acoustic emission method is extremely important for quantitative evaluation due to its ability to register time courses of various acoustic signals, such as the number of counts, amplitude, and energy [7,8,21]. Another important qualitative research method is the use of digital image correlation to assess damage [13,22]. Digital image correlation (DIC) is a non-contact 2D and 3D optical technique using one or more cameras to measure deformation, displacement, vibration, stress, etc. in real time in a single coordinate system. In tests on composite structures, DIC can be used to qualitatively assess defects occurring as a result of static tests, such as bending. Another method that allows for qualitative assessment of composite material damage involves digital microscopy [23,24]. This technique enables more detailed identification of the damaged composite material structure and assessment of damage to composite material fibres/matrix, as well as capturing the delamination phenomenon. When assessing damage to materials, techniques based on thermography or thermal vision are often used [14], although this solution is dedicated to dynamic issues. These relatively new technologies are constantly evolving and provide increasingly sophisticated, non-destructive testing methods for detecting defects such as cavities, cracks, and gaps in materials. These techniques enable the detection of delamination, contaminants, inclusions and porosity. There are, of course, many other techniques for non-destructive testing of composite damage, but this publication presents some of the most commonly used techniques, some of which are employed for experimental investigations.

The bending of thin-walled composite structures has been analysed by many researchers [25–27]. The research presented in this publication involves different aspects to those previously presented in the world literature. The study focused on analysing specific aspects of the behaviour of thin-walled, rectangular cross-section CFRP composite profiles under three-point bending conditions. A novel aspect of the research was the examination of both the positioning of the specimens relative to the supports and the effect of varying support spacing on the structural behaviour, particularly with regard to damage and load-carrying capacity. In terms of the results, it was observed that profiles to which the load was applied via the narrower surface had an average maximum load-carrying capacity that was 1.13 times higher than profiles to which the load was applied via the wider surface. In the context of varying support spacings, it was observed that the highest load-carrying capacity occurred at the smallest support spacing for both types of specimen, regardless of whether the load was applied to the wider or narrower surface. For specimens where the load was applied to the wider surface, the maximum load at a support spacing of 100 mm was 1.21 times higher than at 150 mm. An analogous trend was observed for specimens with the load applied to the narrower surface, with a ratio of 1.15. The initial investigations presenting the possibilities of using non-destructive experimental testing techniques to assess the load-carrying capacity of composite structures subjected to bending were published in the first paper of the research activities conducted in this area [24]. This study comprises a series of research activities that enable the issue of the load-carrying capacity of thin-walled composite columns to be described [28–36], taking into account different variants within the boundary conditions, which represents a certain research novelty.

2. Basic information about the test specimens

The research focused on thin-walled columns with a closed rectangular cross-section made of CFRP composite material. These composite profiles were manufactured using an autoclave technique by the external company WIT-Composites in Poland. The test specimens had identical geometric parameters and composite lay-up. The material used to make the profiles was designated CYCOM 985-42%-HS-135-305 (unidirectional prepreg tape). The resin system was 985 (42% resin) and the fibre type was high strength with a fibre weight of 135 g/m2. All profiles were cured in an autoclave at 177 °C and 0.6 MPa. Further details on the manufacturing of the composite profiles can be found in paper [30]. The material properties were determined in accordance with standards [37–39] The material properties previously determined in accordance with the relevant standards are presented in detail in paper [37]. The material properties of the CFRP material are shown in Table 1.

Table 1. Material properties – average values with standard deviation.

Mechanical Properties		Strength Properties	
Young's modulus E_1 (MPa)	103,014.11 (±2,145.73)	Tensile Strength F_{TU} *(0°)* (MPa)	1,277.41 (±56.23)
Young's modulus E_2 (MPa)	7,361.45 (±307.97)	Compressive Strength F_{CU} *(0°)* (MPa)	572.44 (±46.20)
Poisson's ratio v_{12} [-]	0.37 (±0.17)	Tensile Strength F_{TU} *(90°)* (MPa)	31.46 (±9.64)
Kirchhoff modulus G_{12} (MPa)	4,040.53 (±167.35)	Compressive Strength F_{CU} *(90°)* (MPa)	104.04 (±7.34)
-	-	Shear Strength F_{SU} *(45°)* (MPa)	134.48 (±2.71)

The composite specimens consisted of eight layers of composite material of equal thickness, giving the composite profile walls a total thickness of 1.24 mm. The cross-section of the composite profile was 50x30 mm. The composite profile was 200 mm long. The composite lay-up was $[90°/-45°/45°/0°]_s$. Six composite columns were used in the study. Specimens supported on the wider surfaces of the profile (Sd-1, Sd-2 and Sd-3) are shown in Fig. 1a, while specimens supported on the narrower surfaces (Sd-1x, Sd-2x and Sd-3x) are shown in Fig. 1b. The only difference between the specimens in Figs. 1a and 1b is that the profiles have been rotated by 90° for the purposes of the research described in the research methodology section. All samples have identical dimensions.

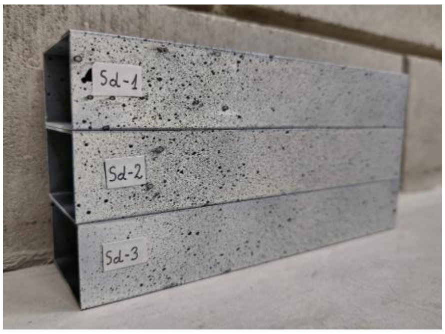

(a)

(b)

Figure 1. Test specimens.

3. Research methodology

The experimental study was conducted to evaluate two different aspects of the research, in order to assess the behaviour of thin-walled composite structures under three-point bending conditions.

The study analysed two key aspects:

- the effect of the sample's positioning in relation to the supports,
- the effect of changing the support spacing, on the behaviour of thin-walled composite structures, particularly in terms of damage and loss of load-carrying capacity.

The first aspect of the study involved analysing samples positioned between supports in two different methods. In the first case, the samples were positioned so that they were supported on the wider surfaces of the profiles. In the second case, the samples were rotated by 90° relative to the initial position, resulting in support on the narrower surfaces of the composite. Fig. 2 illustrates the first aspect of the study in a schematic form, while Fig. 3 shows the actual positioning of the test specimens.

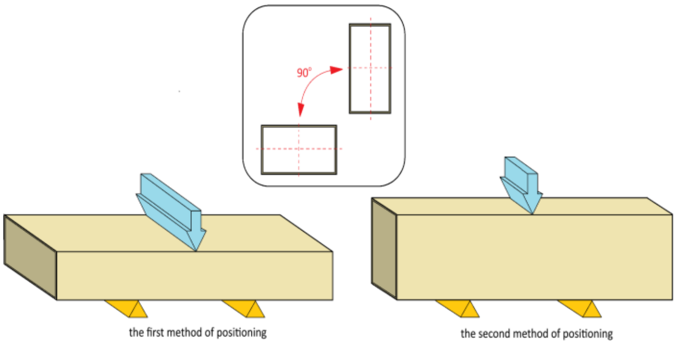

Figure 2. Methods for mounting (positioning) test specimens – schematic presentation.

The second aspect of the study involved analysing the effect that varying support spacing has on the behaviour of structures subjected to bending. Obviously, this aspect applied to samples from both mounting methods. Three support spacing options were considered: 1 – 100 mm, 2 – 125 mm and 3 – 150 mm. The numerical designations (1, 2 and 3) corresponded to the support spacing used. Fig. 4 shows a schematic illustration of variable support spacing, and Fig. 5 shows an example of actual boundary conditions.

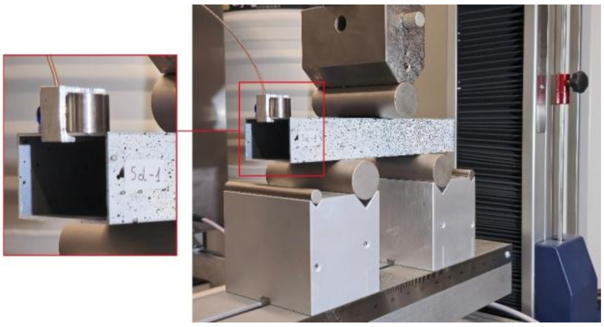

(a)

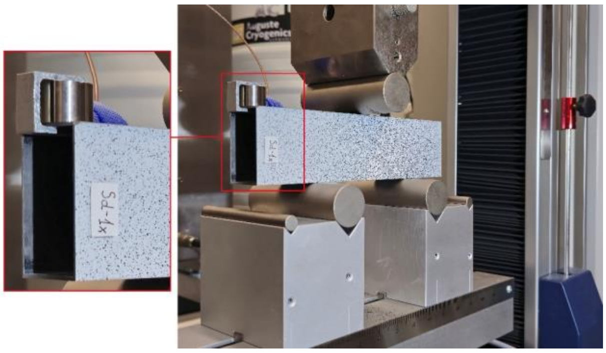

(b)

Figure 3. Actual methods for mounting test specimens: (a) the first option, (b) the second option.

Various research methods were employed to carry out the experimental tests, each of which allowed for the independent evaluation of the bending strength of thin-walled composite columns. The tests were performed using a Cometech QC-505M2F universal testing machine with a maximum load capacity of 50 kN. Three-point bending tests were performed on this apparatus using specialised supports. These tests were conducted at room temperature and at a constant crossbeam speed of 2 mm/min as part of static structural bending strength tests. The tests were carried out in compliance with the standards PN-EN ISO 178 (for plastics) and PN-EN ISO 14125 (for fibre-reinforced composites). The diameter of the supports and the loading component were the same, which was 30 mm.

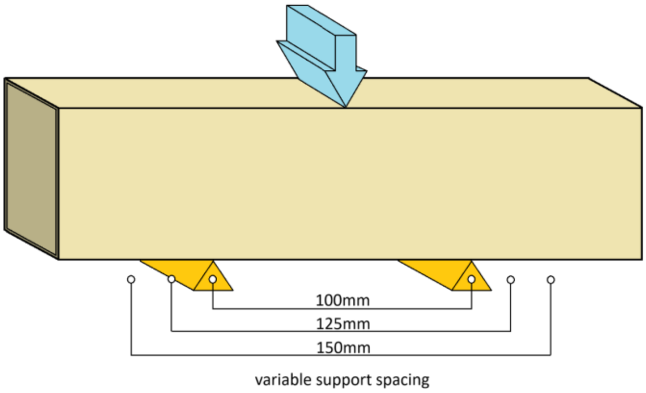

Figure 4. Schematic representation of variable support spacing.

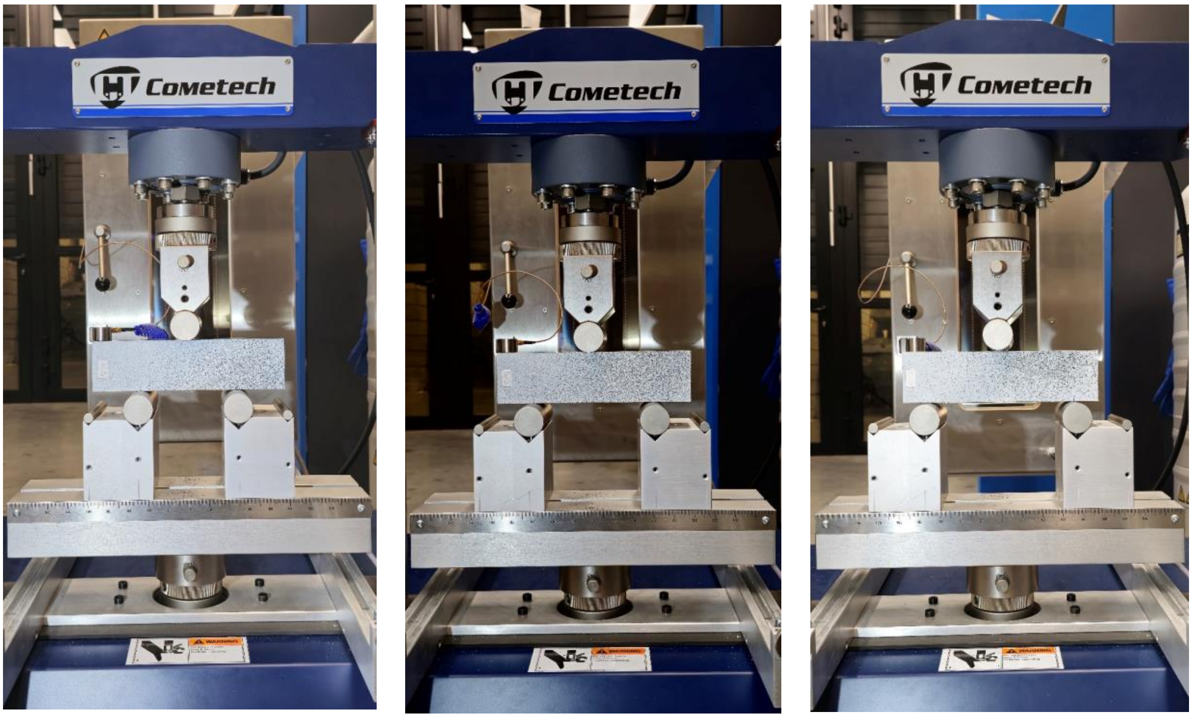

(a) (b) (c)

Figure 5. Actual representation of variable support spacing: (a) 100 mm, (b) 125 mm, (c) 150 mm.

During experimental studies using a universal testing machine (UTM), it was possible to measure the load-displacement characteristics (equilibrium paths during) three-point bending tests. The displacement naturally corresponded to the crosshead displacement of the UTM and was registered using the Amis Plus system, which is compatible with the UTM. Furthermore, non-destructive testing equipment for composite materials was used as part of the research activities. This type of equipment enables additional quantitative and qualitative assessment of the structure's behaviour in static tests. For quantitative assessment, a SpotWave 201 single-channel acoustic emission (AE) system (Vallen Company) was used. This device enabled acoustic signals to be registered (based on the registration of elastic waves in the material), facilitating the evaluation of composite material damage during three-point bending. The VS150-L passive piezoelectric sensor was used to register signals. This sensor is dedicated to testing thin-walled composite structures and aluminium alloys (materials with no ferromagnetic surface), among other things. Both the recording of acoustic signals and the subsequent analysis of the test results were performed using Vallen's dedicated AE software (Vallen Control Panel). Acoustic emission tests were carried out by attaching an acoustic emission sensor to the flat surface of the structure to which it must be permanently connected. During the tests, the energy signal, number of counts and amplitude were primarily measured. The Aramis device for digital image correlation in the basic 2D version was used more for qualitative evaluation of the three-point bending phenomenon. Digital image correlation (DIC) is a procedure used to calculate 2D or 3D coordinates from single images or sequences of images captured using a single camera, a stereo camera, or a multi-camera system. Using a non-contact deformation measurement system makes it possible to measure deformation levels during bending processes and observe critical areas of the structure. DIC enables displacements and deformations to be measured in real time and the deformation process analysed, including the observation of crack propagation, delamination and damage to various materials and structures. In the study, the digital microscope VHX-970F (VHX-7000 series from Keyence Company) was used to assess the structural damage to the material, mainly in a qualitative context. This microscope enabled a qualitative assessment of the damage zone using the depth composition function. This enabled both precise registration of superficial damage to the material structure and registration of the complex nature of damage through the depth of focus of areas slightly distanced from each other. In this study, a VH-Z20T zoom lens with a maximum magnification of 200x was used as the recording head (camera); however, the magnification used during the study was much lower, which was sufficient to visualise the recorded damage. Further information on the digital microscope used in this study can be found in scientific publications on the stability and load-carrying capacity of compressed thin-walled composite profiles [23,30]. Additional measuring devices are shown in Fig. 6.

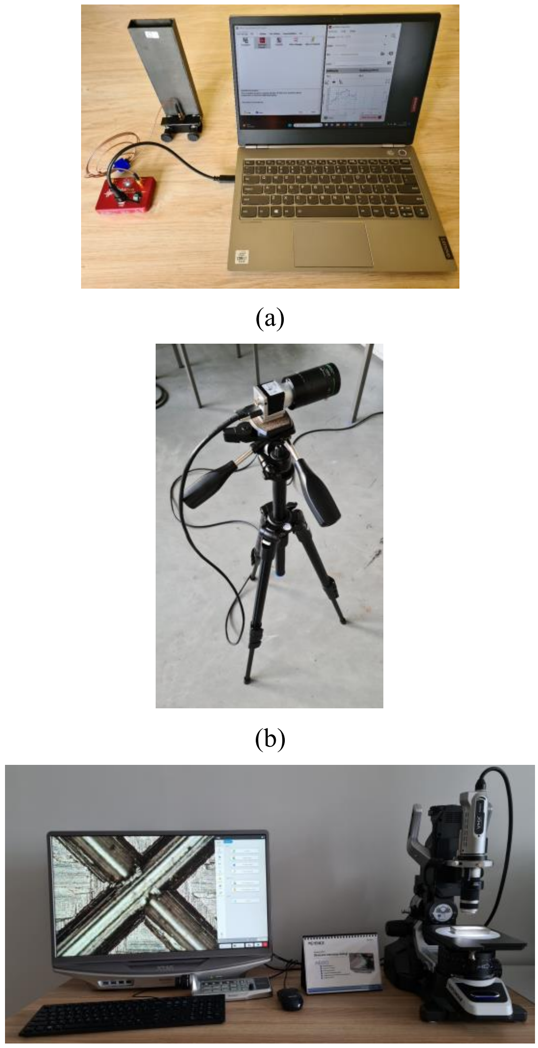

(a)

(b)

(c)

Figure 6. Additional measuring devices: (a) AE system, (b) 2D DIC system, (c) digital microscope.

The universal testing machine used in the study, along with the necessary instrumentation and non-destructive testing systems, enabled the bending capacity of thin-walled composite columns to be tested in depth. This study is part of a series of interrelated research activities, and subsequent stages (future publications) will present the impact of the composite lay-up on the load-carrying capacity of the structure.

4. Research results

The load-carrying capacity of the composite structures was evaluated using a number of independent experimental methods. Initially, load-carrying capacity was assessed using load-displacement curves. Based on these results, a preliminary, general analysis of the behaviour of thin-walled structures was performed. During the initial research stage, the only quantitative comparison made in terms of load-carrying capacity was between the Sd-1, Sd-2 and Sd-3 specimens and the Sd-1x, Sd-2x and Sd-3x specimens. The results relating to the experimental curves obtained from the universal testing machine corresponded to the load directly registered by the machine's testing head, while the displacement corresponded to that of the machine's crosshead (not that of the test specimens directly). Figure 7 shows the characteristics obtained for the test specimens.

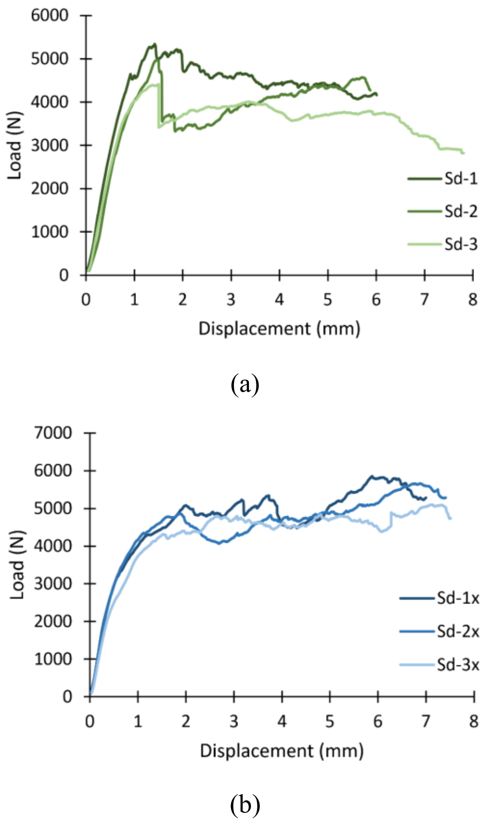

Figure 7. Load-displacement characteristics: (a) specimens loaded relative to a wider surface, (b) specimens loaded relative to a narrower surface.

Based on the tests conducted, it was observed that, for specimens to which the load was applied to a wider surface (Sd-1, Sd-2 and Sd-3), the maximum load occurred in the initial phase of the tests. For specimens to which the load was applied to a narrower surface (Sd-1x, Sd-2x and Sd-3x), the maximum load occurred in the final phase of the tests. The three-point bending phenomenon exhibits a high degree of unpredictability within the recorded test parameters, as illustrated by the load-displacement curves. Despite identical test specimens, there is no clear repeatability of results. This lack of repeatability in the course of the experimental curves highlights the need for more thorough research into the load-carrying capacity of composite structures. Based on the determined characteristics (Fig. 7), the maximum load values were determined and considered as failure loads. Table 2 summarises the maximum load values recorded during three-point bending tests.

Table 2. Limit loads.

First positioning variant			Second positioning variant		
Sd-1	5340.41N	Avg= 4907.89N	Sd-1x	5851.20N	Avg= 5537.53N
Sd-2	4972.90N		Sd-2x	5663.06N	
Sd-3	4410.36N		Sd-3x	5098.32N	

The maximum load values for the first positioning variant (specimens Sd-1, Sd-2 and Sd-3) were lower than those for the second positioning variant. In fact, the average limit load value for the second positioning variant is 1.13 times higher than that for the first. For both positioning variants, it was observed that as the distance between the supports increased, the limit load decreased. For the first positioning variant, the maximum load for specimen Sd-1 relative to Sd-3 was 1.21 times higher. For the second positioning variant, the maximum load for specimen Sd-1x relative to Sd-3x was 1.15 times higher. Despite the maximum load values being reached, followed by a decrease in load value, the course of the load was characterised by high irregularity. This underlines the importance of conducting more detailed research into the load-carrying capacity of thin-walled composite structures subject to bending. Based on the tests conducted, a trend was verified whereby the limit load value decreased for both specimen positioning variants as the distance between the supports increased – Fig. 8.

In the case of the first positioning variant of the test specimens, it was estimated that there was an almost linear trend, as indicated by the trend line. In contrast, a larger deviation from the linear trend was observed in the case of the second positioning variant. For the first variant (Fig. 8a, for specimens Sd-1, Sd-2 and Sd-3), the correlation coefficient between the specimens and the trend line was found to be $R^2 = 0.9856$. For the second variant (Fig. 8b, for specimens Sd-1x, Sd-2x and Sd-3x), the correlation coefficient was significantly lower, at $R^2 =$

0.923. This confirms that when the load is applied in accordance with the first positioning variant (where the specimens are loaded on a wider surface), a relatively linear trend is observed in terms of the decrease in limit load relative to the increase in distance between supports. In the second positioning variant, where the load is applied to a narrower surface, a more significant deviation from linearity was observed as the limit load decreased with an increase in the distance between the supports. This indicates more irregular and unpredictable behaviour. This is related to the fact that damage in the first positioning variant occurred due to the lower stiffness of the profile resulting from its arrangement in relation to the supports. The load course in the first (Fig. 7a) and second (Fig. 7b) positioning variants was completely different. In the first case, maximum loads were observed at the beginning of the load course; in the second case, maximum loads were observed at a much later stage of loading.

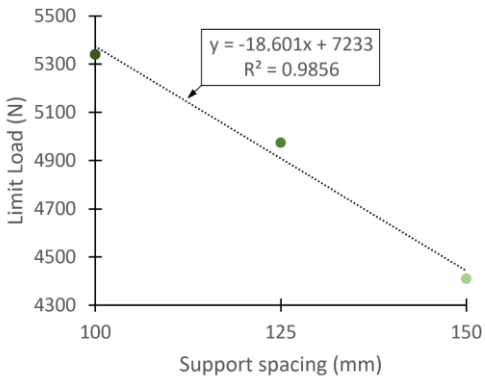

(a)

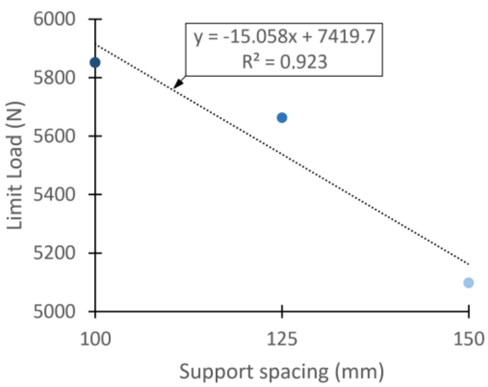

(b)

Figure 8. Effect of limit load on the change of support spacing: (a) first positioning variant (3 specimens), (b) second positioning variant (3 specimens).

Due to the irregularity of the load-displacement characteristics, a more detailed analysis of the structure's behaviour under three-point bending was conducted using the acoustic emission method. Acoustic emission (AE) is the generation and propagation of elastic waves in a material during sudden, localised changes to its structure, such as cracking, friction or plastic deformation. In technical diagnostics, several basic stages of acoustic emission can be identified: 1) damage source, 2) wave generation, 3) propagation, 4) detection, 5) analysis, 6) diagnosis. Using this method made it possible to perform a quantitative assessment of the damage to composite material, which is a complex phenomenon. Using the acoustic emission method enabled a detailed analysis of damage to composite structures subjected to bending, allowing for a more accurate interpretation of the irregular course of the experimental load-displacement curves. Different acoustic signals were initially used as part of the acoustic emission method, such as energy, amplitude, number of counts and sum of counts — example results are presented in Fig. 9. In Fig. 9, the red lines show the curves representing the course of selected acoustic emission signals, while the second colour shows the course of the load curves.

From the acoustic emission signals presented in Fig. 9, the energy signal and the sum of counts were selected for further analysis to provide the most accurate interpretation of composite material damage. Two specific signals (energy and sum of counts) were selected for analysis as the others did not permit clear identification of significant changes during the bending phenomenon. The amplitude signal was omitted from the analysis because the signal values remained very high for practically the entire duration of the tests, almost from the very beginning of the bending phenomenon. The count signal was also omitted due to its similarity to the energy signal, despite the difference in values. Due to the complex nature of the progressive damage process, the amplitude signal showed extremely high intensity and was not analysed in detail in this study. To evaluate the level of damage to composite structures, the two aforementioned signals — energy and sum of counts — were used, as these distinct signals allow for the independent interpretation of results in comparison with load-displacement curves. In the case of the energy signal, local 'peaks' in the signal were evaluated, which potentially indicated further symptoms of permanent damage, while an increase in the sum of counts signal was observed from a certain 'linear' level, which occurred only in the initial stage. Figs. 10 and 11 show the acoustic signals compared with the experimental load-displacement curves for all test specimens.

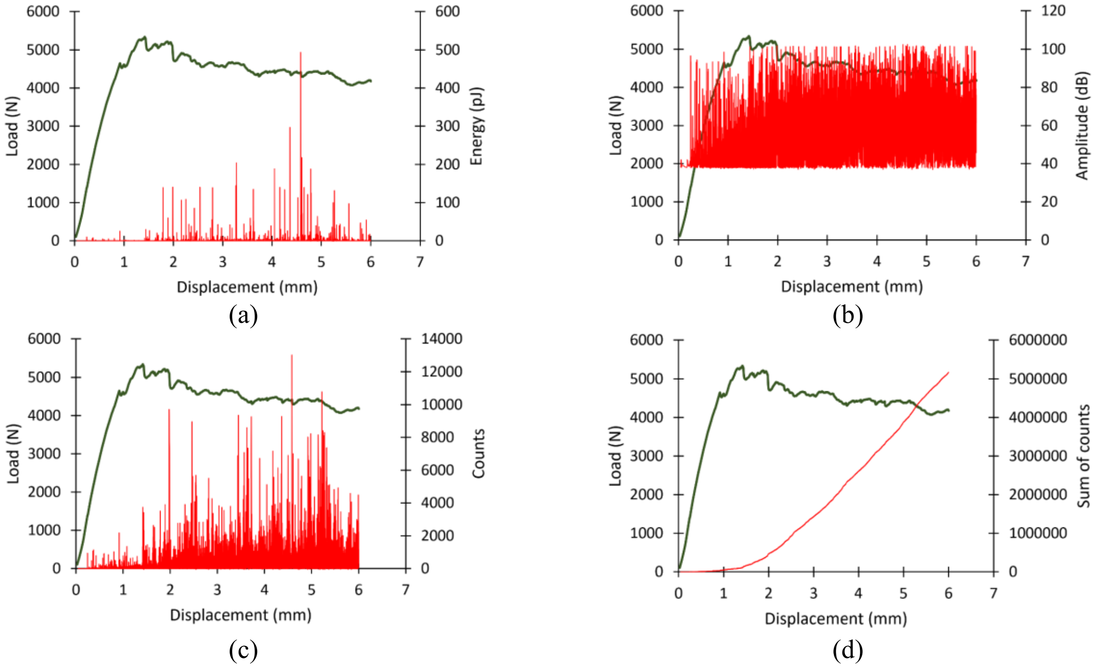

Figure 9. Example results from the use of AE: (a) energy, (b) amplitude, (c) counts number, (d) counts sum.

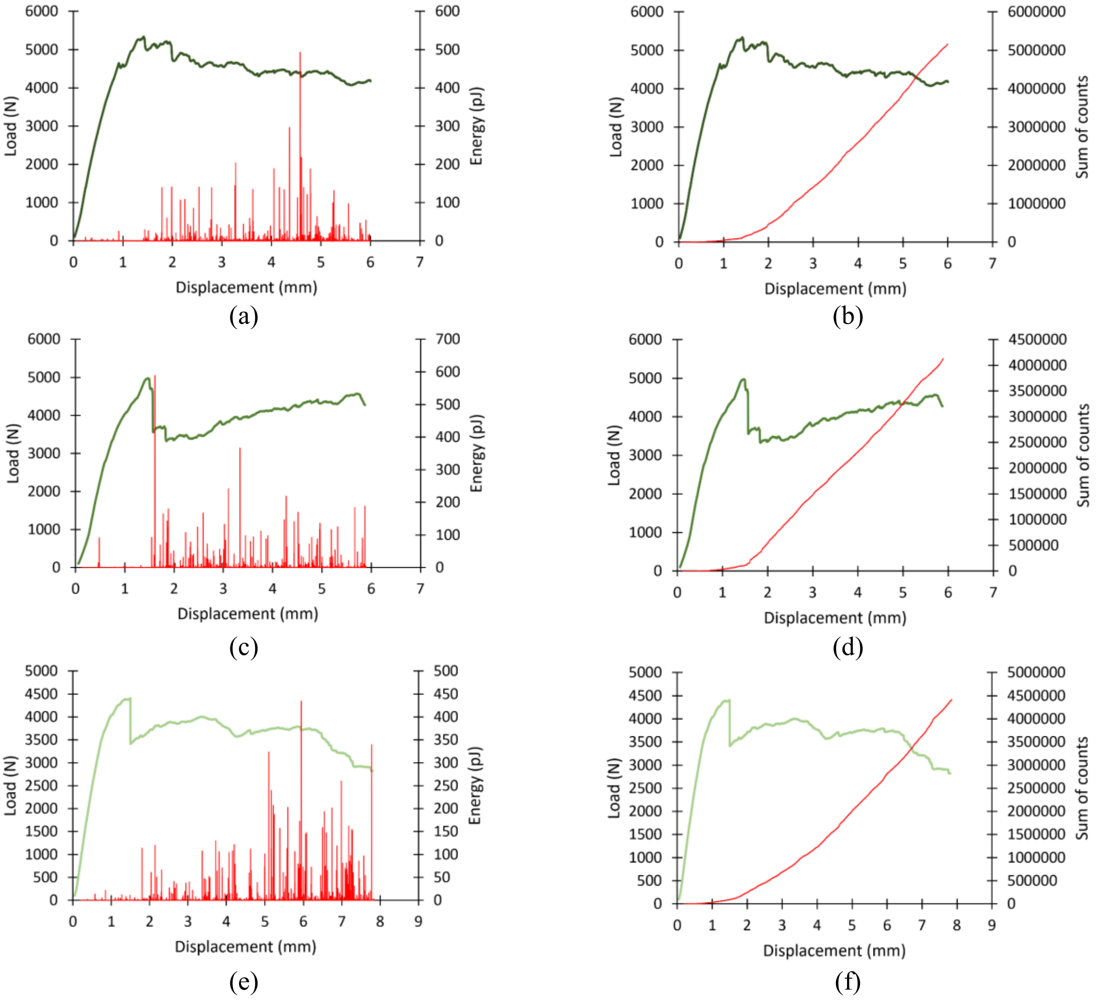

Figure 10. Load-displacement characteristics with AE signals: (a,b) specimen Sd-1, (c,d) specimen Sd-2, (e,f) specimen Sd-3.

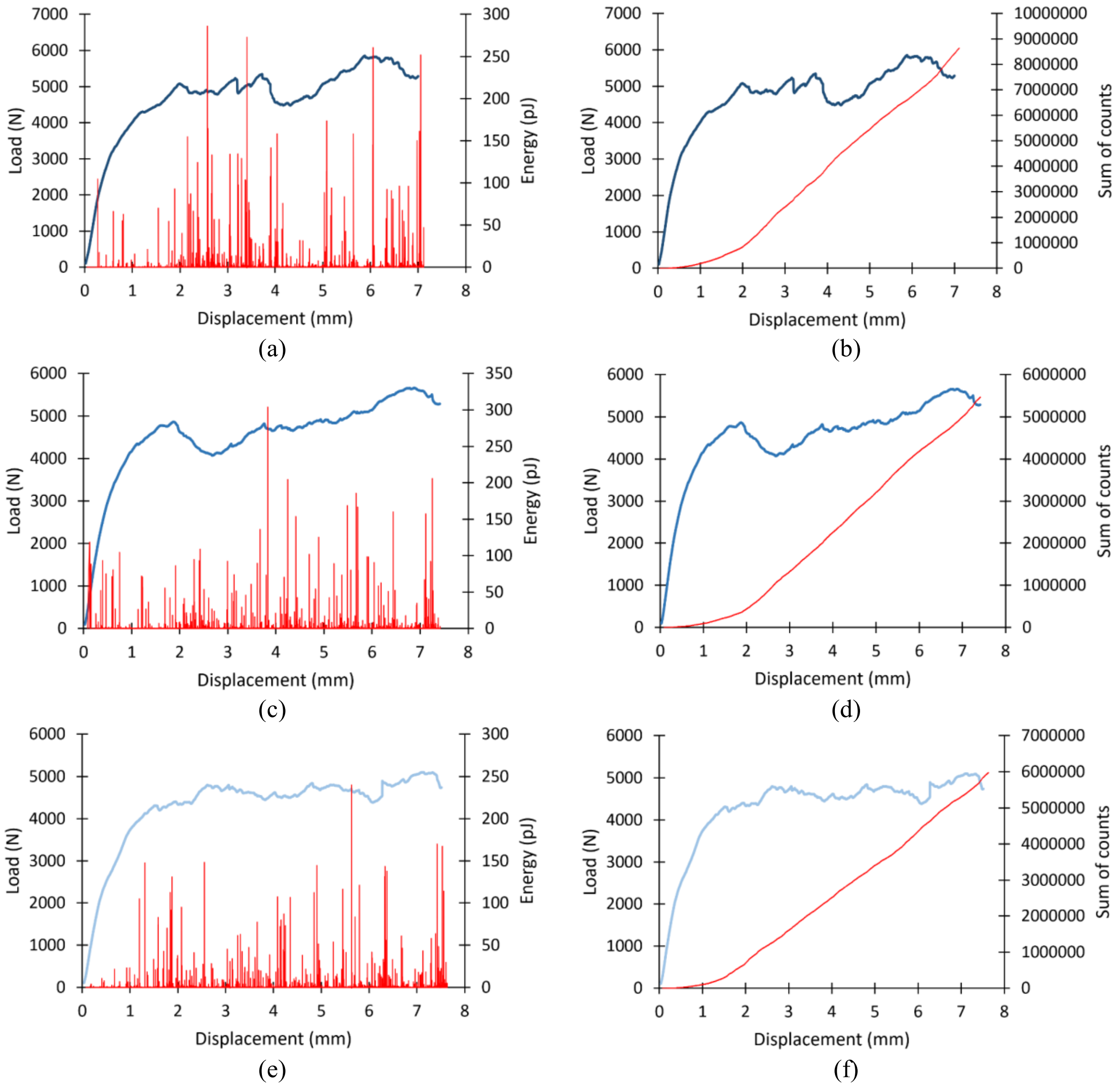

Figure 11. Load-displacement characteristics with AE signals: (a,b) specimen Sd-1x, (c,d) specimen Sd-2x, (e,f) specimen Sd-3x.

Tests conducted using acoustic emission made it possible to analyse the results in relation to the load-displacement characteristics. During the tests, it was observed that an energy signal reaching (or exceeding) 100 pJ was most often associated with changes in the load-displacement characteristics. During the test trials, locally occurring 'peaks' in the energy signal of up to several hundred pJ were also recorded. In the case of the three-point bending phenomenon, damage to the composite material structure was observed to be a relatively long-lasting and complex process, as evidenced by numerous increases and decreases in the energy signal. Energy signal increases were usually observed during the recording of maximum loads. Irregularities in the load-displacement curves, along with corresponding increases and decreases in the energy signal, indicate the progressive damage to the composite material during the experimental tests. Specimens from the first positioning variant (Sd-1, Sd-2 and Sd-3) showed a maximum load value at approximately 1.5 mm displacement, whereas specimens from the second positioning variant (Sd-1x, Sd-2x and Sd-3x) showed a maximum load value at approximately 6–7.5 mm displacement. Specimens from the first positioning variant showed no significant increases in the energy signal at the initial stage of loading (until approximately 1.5 mm of displacement), indicating that material damage occurred at a later stage of loading. In contrast, increases in the energy signal were observed almost from the initial stage of loading in the case of specimens from the second positioning variant, indicating the progression of damage from the beginning of the tests. The locally registered energy signal peaks, at approximately 350–600 pJ for the first positioning variant and

150–350 pJ for the second positioning variant, show significant changes in load characteristics when compared with the load-displacement curves. The difference in energy signal intensity between the two variants indicates that the damage phenomenon is significantly more complex in the case of the second variant. An acoustic emission signal indicating the sum of counts showed a rapid increase in value after only about 1 mm of displacement. This suggests that the composite material began to undergo a complex damage process at such an early stage of the three-point bending test. After exceeding 2 mm of displacement, a relatively regular course of the acoustic emission signal indicating the sum of counts (similar to a linear signal) was also observed during the tests. This indicated a certain stabilisation of the test specimens in terms of the progression of the damage. The specimens in the first and second positioning variants demonstrated lower and higher stiffness, respectively, resulting from the positioning method shown in Fig. 2.

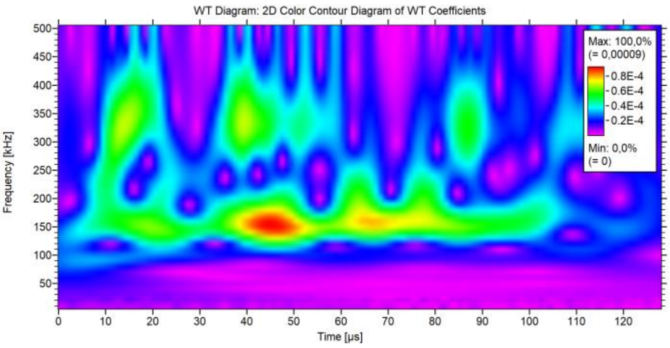

(a)

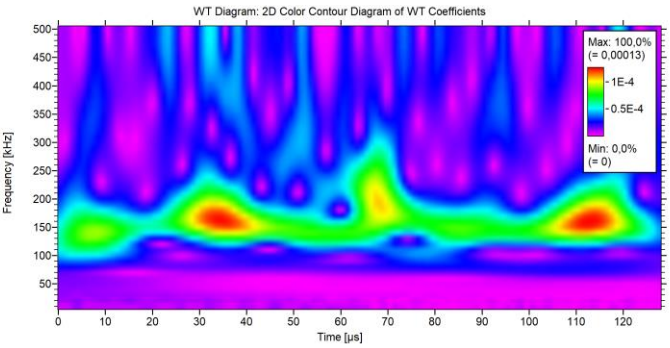

(b)

Figure 12. WT diagram (AE): (a) specimen Sd-1, (b) specimen Sd-1x.

Moreover, example results relating to the use of the wavelet transform (WT) scalograms of the acoustic emission (AE) signal for CFRP composite material are presented. The graphs in Fig. 12 relate to samples Sd-1 and Sd-1x from the first and second mounting (positioning) variants, respectively. The diagram illustrates the distribution of AE signal energy over time and frequency.

In the analysed cases (Fig. 12), the highest energy values correspond to the red and yellow areas. In the analysed signal – specimen Sd-1 (Fig. 12a), mid-frequency ranges of approximately 130–180 kHz dominate, alongside local high-frequency events at 250–400 kHz and continuous low-frequency activity below 100 kHz. In acoustic emissions from CFRP composites, individual frequency ranges are typically associated with specific degradation mechanisms. The 50–120 kHz range may be associated with interlaminar friction, delamination propagation, contact effects, and structural damping. The graph shows continuous activity in this range throughout most of the measurement period, which could indicate progressive delamination or propagation of existing interlaminar damage. The strongest energy occurs at approximately 40–50 µs with a frequency of around 150–170 kHz. The most likely phenomena are fracture of the epoxy matrix, initiation of microcracks and local delamination. This is probably the main failure event in the analysed waveform. In the 250–400 kHz range, short-duration, high-frequency peaks occur at approximately 10–20 µs, 35–50 µs and 80–90 µs. In CFRP, such frequencies are often associated with carbon fibre breakage, sudden energy release and localised crushing of fibres. As these signals are short and pulsed, they can be interpreted as individual events of brittle fibre damage. WT analysis suggests that the CFRP material under investigation underwent multi-mechanism damage. The most critical event occurs at approximately $t \approx 45$ µs and $f \approx 160$ kHz, which corresponds to the maximum concentration of acoustic emission energy.

In the analysed signal – specimen Sd-1x (Fig. 12b), certain similarities and differences were observed compared with specimen Sd-1. The scalogram of the wavelet transform of the acoustic emission signal for the CFRP material (Fig. 12b) indicates a dominant concentration of energy in the 150–170 kHz range, with two main peaks at approximately 35 µs and 113 µs. This dominant energy concentration in the form of a mid-frequency peak, coupled with the local broadening of the range to 250–300 kHz, suggests the presence of matrix-interlaminar damage, including matrix cracking, fibre-matrix debonding, and delamination. The absence of a strong, distinct peak above 300 kHz suggests that fibre fracture is not the primary source of the analysed signal. Similarly, the contribution of low-frequency phenomena below 100 kHz, such as friction, contact and global vibrations, or some matrix damage, is negligible.

In the literature, the assignment of frequency ranges to damage mechanisms is not absolute, but the general rule is: lower ranges for matrix cracking/damage, mid-range for delamination, and higher ranges for fibre fracture. In practice, the WT graph acts as a 'micro-time damage seismograph': it shows in which frequency ranges the AE wave energy packets appear. CWT methods are used in materials such as CFRP to identify and localise damage, including matrix cracking, delamination and fibre damage, based on the dominant frequency range.

The complexity of the damage phenomenon required additional experimental methods, such as digital image correlation (DIC), to be used. Using an optical deformation measurement system (Aramis), which was based on digital image correlation, information on the deformation level (strain in the vertical direction) for the tested structures was obtained. It was observed that the maximum deformation level occurred just below the element loading the composite structures and that the deformation distribution progressed vertically, in accordance with the direction of the three-point bending tests (see Fig. 13).

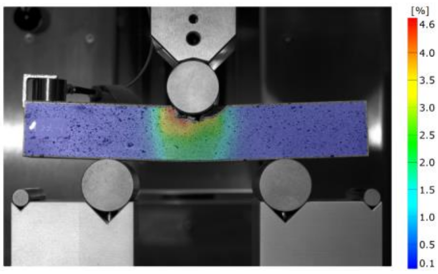

(a)

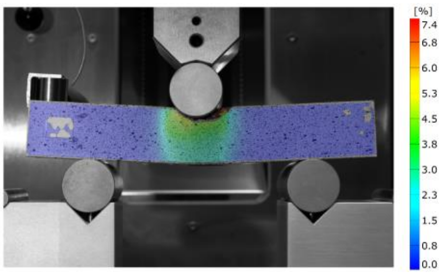

(b)

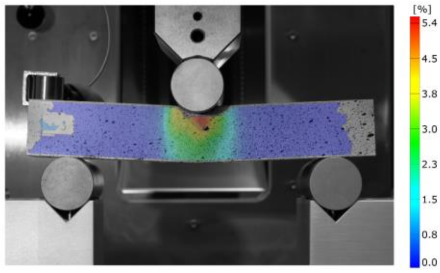

(c)

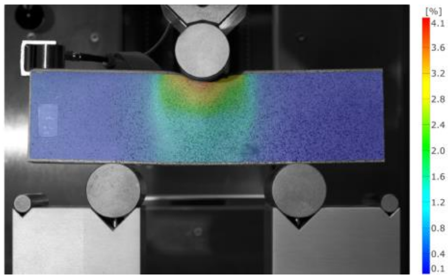

(d)

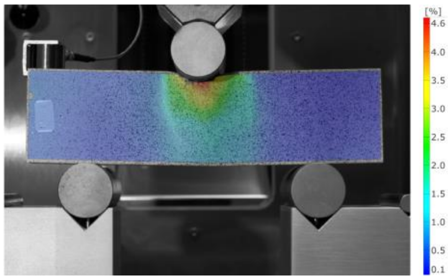

(e)

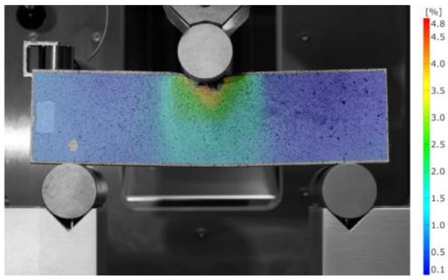

(f)

Figure 13. Deformations registered using digital image correlation: (a) specimen Sd-1, (b) specimen Sd-2, (c) specimen Sd-3, (d) specimen Sd-1x, (e) specimen Sd-2x, (f) specimen Sd-3x.

The results obtained from measuring the deformation level (strain in the vertical direction of the structure) are presented for both the first (Fig. 13a, b, c) and second (Fig. 13d, e, f) positioning variants of composite structures. It was observed that, in both cases, the distribution of deformation (strain) in the vertical direction was relatively similar. However, in the first case, i.e. for the specimens from the first positioning variant, the strain values were slightly higher. The results shown in Figure

13 indicate the level of deformation expressed as a % of strain. For the specimens with the first mounting variant, maximum strains ranging from 4.6% to 7.4% were observed. For the specimens with the second mounting variant, strains between 4.1 and 4.8% were recorded. The dominant areas of damage (marked in red) were located just below the element loading the structures. Due to the significantly more intense level of damage observed in the specimens from the first positioning variant, a more in-depth analysis of the results was conducted using a high-precision digital microscope (in particular the depth of field option).

Figure 14 shows the damage to the specimens from the first (Fig. 14a) and second (Fig. 14b) positioning variants, where the support spacing was 100 mm.

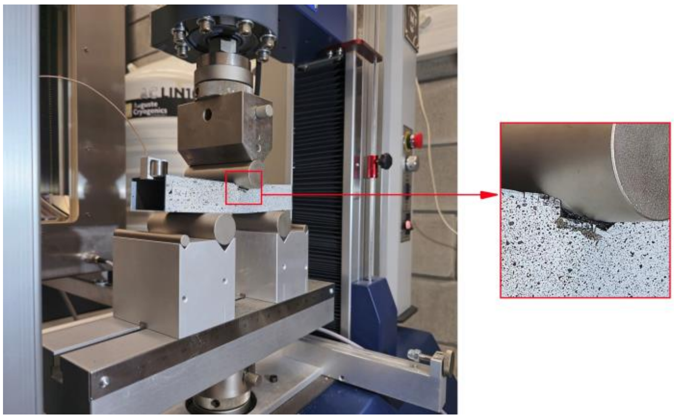

(a)

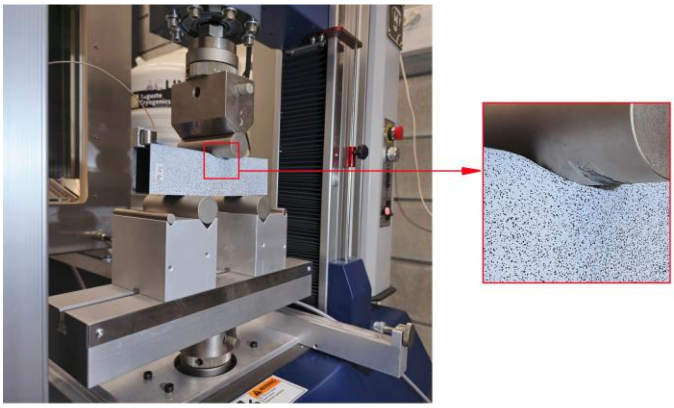

(b)

Figure 14. Form of structural damage: (a) specimen Sd-1, (b) specimen Sd-1x.

Specimens from the first positioning variant (Sd-1, Sd-2 and Sd-3) demonstrated more visible damage.

In order to more precisely visualise the damage, digital microscopy was used for both the first and second positioning variants. This enabled the damaged areas of the structure and the complex forms of damage to the composite material to be observed more effectively – Fig. 15. Additionally, it was possible to demonstrate the influence of support spacing on damage to the test specimens in both positioning variants.

(a)

(b)

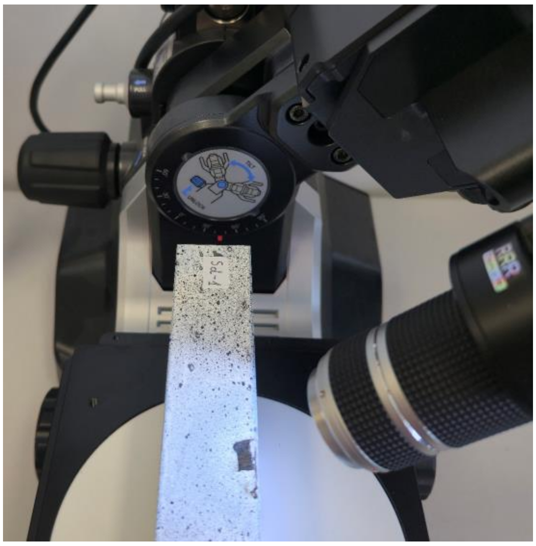

(c)

Figure 15. Inspection of damaged areas using digital microscopy: (a) full inspection set-up, (b) VHX-970F digital microscope with mobile inspection head, (c) detailed view of the inspection method at a 45°.

Above all, the use of digital microscopy enabled a qualitative assessment in the context of correctly interpreting the forms of damage registered on the composite material. The microscope head was set at a tilt angle of 45° relative to the edge where the dominant forms of damage were observed as a result of loading the composite profiles. This tilt angle allowed damage to be observed not only on the side surface of the specimen, where the dominant forms of damage were observed, but also on the top surface, which was subjected to load during the three-point bending tests. The results showing the damaged areas obtained are presented in Fig. 16 at a magnification of 20x.

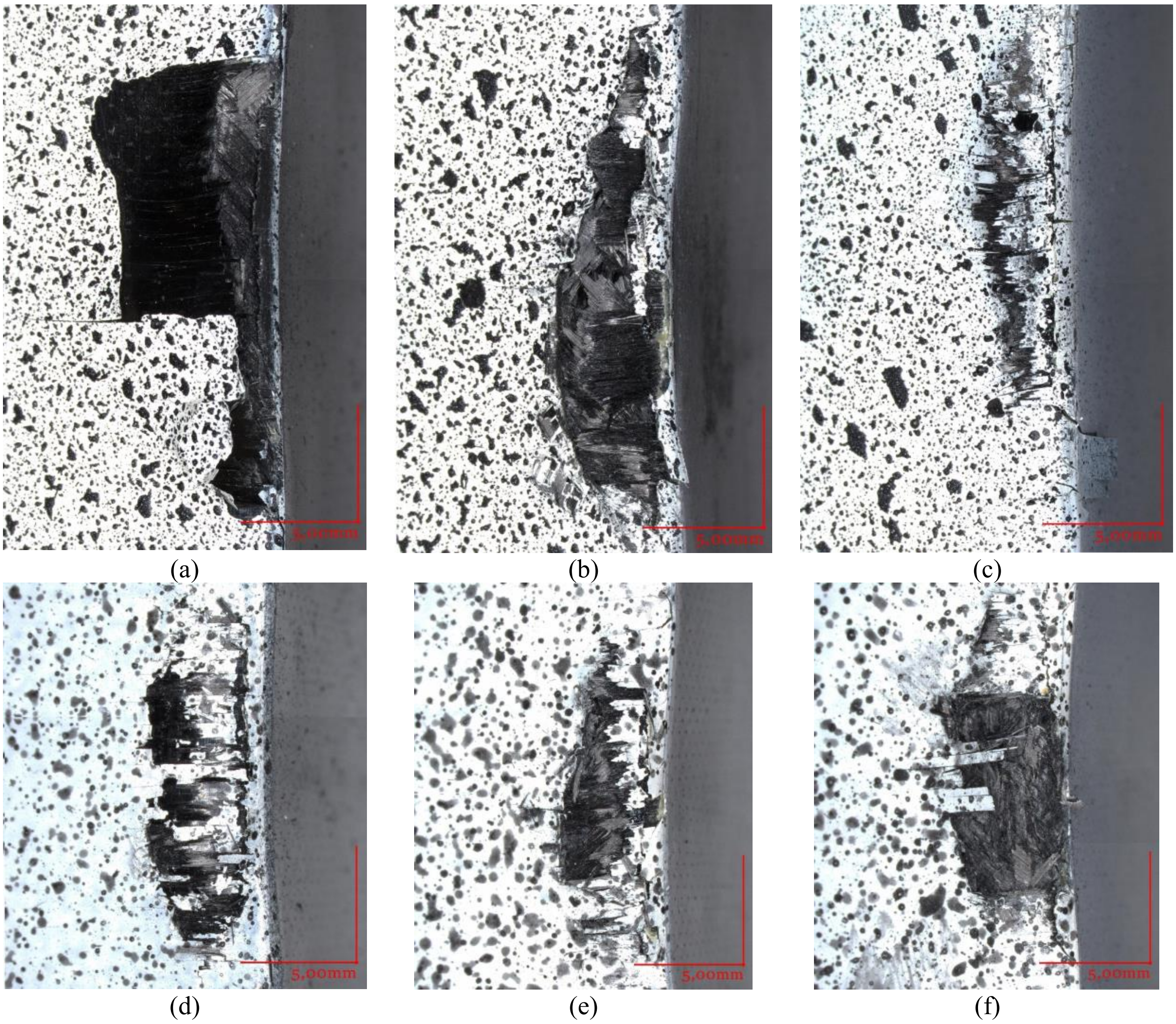

Figure 16. Damage areas of individual specimens from both positioning variants: (a) specimen Sd-1 (first positioning variant), (b) specimen Sd-2 (first positioning variant), (c) specimen Sd-3 (first positioning variant), (d) specimen Sd-1x (second positioning variant), (e) specimen Sd-2x (second positioning variant), (f) specimen Sd-3x (second positioning variant).

Based on the results of the tests conducted, it was observed that the damage areas were significantly smaller in the first positioning variant (Sd-1, Sd-2, Sd-3) than in the second (Sd-1x, Sd-2x, Sd-3x). The size of the damaged area decreased significantly with increasing support spacing. A microscope with magnifications of 20x, 50x and 100x was used to assess the damage, enabling a thorough evaluation of the complex forms of damage to the composite material structure (see Fig. 17).

It was observed that complex forms of damage, such as delamination and cracking of layers (and individual fibres), occurred in both the first and second positioning variants. The first positioning variant showed more extensive damage in terms of area than the second positioning variant, as confirmed by Figures 16 and 17. All results obtained using digital microscopy were presented using an advanced function that allowed damage forms to be registered using the depth of field option. Several characteristic failure mechanisms typical of CFRP laminates subjected to mechanical loading can be identified based on the presented micrographs of a composite layup $[90/-45/45/0]_s$. Distinct areas of delamination are visible between adjacent laminate layers, particularly in the boundary zones between layers with different fibre orientations. Microscopic examination shows local layer separation, interlaminar separations, irregular separation boundaries and damage propagation along the interfaces. Intense delamination occurs at the ±45° layer boundaries, near the 0° layers and in stress concentration zones. This is due to differences in stiffness between layers with different orientations, shear stresses between layers and degraded matrix–fibre adhesion. Numerous cracks are visible within the individual composite layers. The characteristics of the damage pattern for the fractures include: fractures running parallel to the fibre direction; local matrix fragmentation; transverse microcracks; and damage propagation from the edges towards the interior of the laminate. The 50× and 100× micrographs reveal cracks in the diagonal layers, cracking of the epoxy matrix and zones of brittle fracture. The most susceptible layers are: ±45°, where shear stresses dominate, and 90°, where cracks occur transversely to the fibres. Signs of degradation of the fibre reinforcement itself are also visible. The observed forms of damage are: fibre cracking, fibre pull-out from the matrix, local buckling and crushing of fibre bundles and delaminated fibre strands. At the highest magnification (100×), discontinuity of the fibres, as well as frayed fibre ends and areas of loss of fibre-matrix cohesion, can be observed.

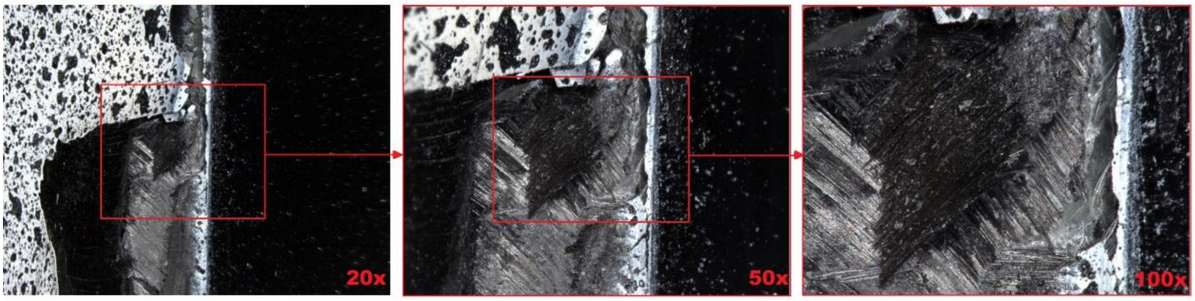

(a)

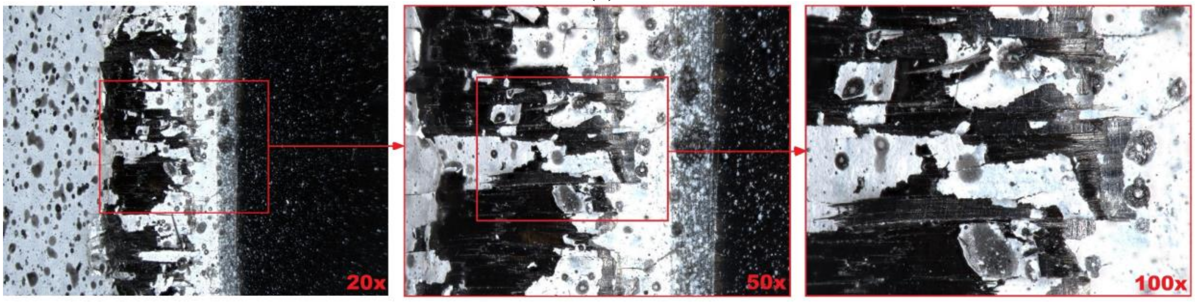

(b)

Figure 17. Damaged areas with demonstration of material failure forms for selected test specimens: (a) specimen Sd-1 (first positioning variant), (b) specimen Sd-1x (second positioning variant).

The analysed composite exhibits a multi-mechanism degradation process including initiation of matrix microcracks, development of interlaminar cracks and delamination. The applied layer sequence $[90/-45/45/0]_s$ results in: high stress concentrations at the interfaces of layers with varying orientations; the development of shear stresses between the ±45° and 0° layers; and delamination propagating through the thickness of the laminate. The dominant failure mechanisms of the tested composite are interlaminar delamination and matrix cracking. Fibre damage occurs at a more advanced stage of degradation and indicates a loss of the laminate's load-carrying capacity.

Furthermore, to assess the damage more comprehensively in qualitative terms, the damage areas were visualised in three dimensions to allow consideration of the depth of the damage area. Contour maps were used for this purpose, enabling damage to be assessed in a direction perpendicular to the analysed damage areas, as shown in Figure 18, which illustrates this process using example specimens. The results shown in the figure below were obtained using 30x magnification.

The microscope used for the research allowed damage to be observed in both the plane of observation and in the direction perpendicular to it, enabling special 3D maps of the damaged area to be generated. This approach allowed for a more detailed presentation of the damaged areas. It was observed that the forms of damage registered in the direction perpendicular to the observed surface (such as layer cracking and progressive delamination) were more significant in the first positioning variant of the test specimens. The results presented in Fig. 18 show the test specimens to be most susceptible to damage at the smallest support spacing. In other cases, the damage phenomenon was significantly smaller. Based on all results obtained from digital microscopy, it was observed that damage occurred just below the point at which the bending load was applied. Regardless of the specimen positioning variant, all forms of damage were observed on the side surfaces of the test specimens. No significant damage to the composite material structure was observed on the upper surface to which the load was applied.

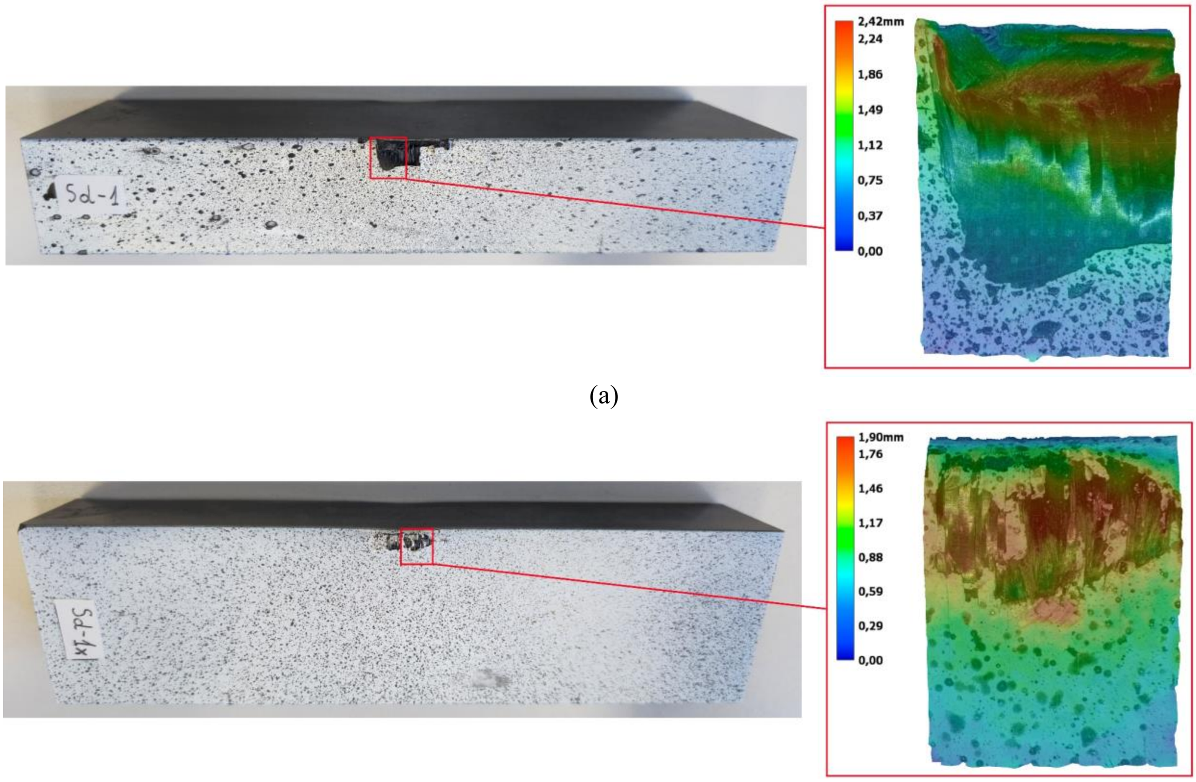

(b)

Figure 18. Damaged areas with demonstration of material failure forms for selected test specimens: (a) specimen Sd-1 (first positioning variant), (b) specimen Sd-1x (second positioning variant).

5. Conclusion

The tests conducted are a type of experimental study that evaluates the load-carrying capacity of thin-walled composite structures under three-point bending conditions. This paper presents an evaluation of the influence of positioning methods on the load-carrying capacity of structures, together with an assessment of composite material damage.

These interdisciplinary experimental research methods enabled a preliminary assessment of the load-carrying capacity of thin-walled composite profiles to be made. The following conclusions were formulated:

- It was estimated that the average failure load for the specimens from the second positioning variant (Sd-1x, Sd-2x and Sd-3x) was 1.13 times higher than that for the specimens from the first positioning variant (Sd-1, Sd-2 and Sd-3).
- The maximum load for specimens with the smallest support spacing (100 mm) was noticeably higher than for specimens with the largest support spacing (150 mm): 1.21 times higher for the first mounting variant and 1.15 times higher for the second.
- It was proven that the maximum load in the first positioning variant specimens occurred in the initial phase of loading the structure, whereas in the second positioning variant specimens, it occurred in the final phase.
- The decrease in limit load relative to the increase in support spacing shows an almost linear trend in the first

positioning variant ($R^2 \approx 0.99$), whereas the second positioning variant shows a higher deviation from linearity ($R^2 \approx 0.92$).

- The high intensity of the acoustic signals, particularly the energy, suggests a complex damage mechanism, possibly involving matrix-interlaminar damage such as matrix cracking, fibre-matrix debonding and delamination.
- The samples from the first mounting variant exhibited higher deformations (4.6%–7.4%), while the samples from the second mounting variant exhibited lower deformations (4.1%–4.8%).
- It was observed that much more extensive damage areas occurred in the first positioning variant specimens.

Observed damage included fibre cracking, pull-out, local buckling, crushing of fibre bundles, and delamination. At 50x and 100× magnification, fibre discontinuities, frayed ends, and loss of fibre–matrix cohesion were visible. The most susceptible layers were ±45° (dominant shear stresses) and 90° (transverse cracking). The combined use of acoustic emission and digital image correlation methods enabled a comprehensive analysis of the damage process in the CFRP composite during loading. Acoustic emission allowed material degradation mechanisms to be detected and identified in real time, while digital image correlation enabled strain distribution to be observed and strain concentration zones to be localised on the specimen surface. The next stage of the research will involve assessing the impact of composite lay-ups on the load-carrying capacity of structures with variable support spacing. Further studies will analyse the influence of composite lay-up (layer arrangement) on the load-carrying capacity of structures in more detail, using one positioning (mounting) variant with various support spacings.

Acknowledgment

The research was conducted under project No. 2021/41/B/ST8/00148, financed by the National Science Centre, Poland.

References

1. Fascetti A, Feo L, Nistic N, Penna R. Web-flange behavior of pultruded GFRP I beams: a lattice model for the interpretation of experimental results. *Composites Part B Engineering* 2016; 100: 257-269. https://doi.org/10.1016/j.compositesb.2016.06.058.
2. Berardi VP, Perrella M, Feo L, Cricrì G. Creep behavior of GFRP laminates and their phases: experimental investigation and analytical modeling. *Composites Part B Engineering* 2017; 122: 136-144. https://doi.org/10.1016/j.compositesb.2017.04.015.
3. Kubiak T, Kolakowski Z, Swiniarski J, Urbaniak M, Gliszczynski A. Local buckling and post-buckling of composite channel-section beams – numerical and experimental investigations. *Composites Part B Engineering* 2016; 91: 176-188. https://doi.org/10.1016/j.compositesb.2016.01.053.
4. Rozylo P. Experimental-numerical test of open section composite columns stability subjected to axial compression. *Archives of Materials Science and Engineering* 2017; 84(2): 58-64. https://doi.org/10.5604/01.3001.0010.0979.
5. Kolanu NR, Raju G, Ramji M. A unified numerical approach for the simulation of intra and inter laminar damage evolution in stiffened CFRP panels under compression. *Composites Part B Engineering* 2020; 190: 107931. https://doi.org/10.1016/j.compositesb.2020.107931.
6. Banat D, Mania RJ. Failure assessment of thin-walled FML profiles during buckling and postbuckling response. *Composites Part B Engineering* 2017; 112: 278-289. https://doi.org/10.1016/j.compositesb.2017.01.001.
7. Rozylo P. Failure phenomenon of compressed thin-walled composite columns with top-hat cross-section for three laminate lay-ups. *Composite Structures* 2023; 304: 116381. https://doi.org/10.1016/j.compstruct.2022.116381.
8. Rozylo P, Debski H. Failure study of compressed thin-walled composite columns with top-hat cross-section. *Thin-Walled Structures* 2022; 180: 109869. https://doi.org/10.1016/j.tws.2022.109869.
9. Li ZM, Qiao P. Buckling and postbuckling behavior of shear deformable anisotropic laminated beams with initial geometric imperfections subjected to axial compression. *Engineering Structures* 2015; 85: 277-292. https://doi.org/10.1016/j.engstruct.2014.12.028.
10. Madukauwa-David ID, Drissi-Habti M. Numerical simulation of the mechanical behavior of a large smart composite platform under static loads. *Composites Part B Engineering* 2016; 88: 19-25. https://doi.org/10.1016/j.compositesb.2015.10.041.
11. Ding F, Cai Y, Tu W, Chen Q, Peng M, Ouyang F, Cai H, Fan K, Zhou W. Research on ultrasonic non-destructive detection method for defects in GFRP laminates based on machine learning. *Ocean Engineering* 2025; 327: 120972. https://doi.org/

10.1016/j.oceaneng.2025.120972.
12. Zhao Y, Zhang Y, Wang J, Yue Q, Chen H. Comparison of non-destructive testing methods of bolted joint status in steel structures. *Measurement* 2025; 242: 116318. https://doi.org/10.1016/j.measurement.2024.116318.
13. Golewski P, Sadowski T, Kneć M, Budka M. The effect of thermal aging degradation of CFRP composite on its mechanical properties using destructive and non-destructive methods and the DIC system. *Polymer Testing* 2023; 118: 107902. https://doi.org/10.1016/j.polymertesting.2022.107902.
14. Katunin A, Pivdiablyk I, Gornet L, Rozycki P. A hybrid method for determination of fatigue limit and non-destructive evaluation of composite structures after low-velocity impact loading. *Composites Part B Engineering* 2022; 238: 109898. https://doi.org/10.1016/j.compositesb.2022.109898.
15. Gliszczynski A, Kubiak T. Load-carrying capacity of thin-walled composite beams subjected to pure bending. *Thin-Walled Structures* 2017; 115: 76-85. https://doi.org/10.1016/j.tws.2017.02.009.
16. Kazmierczyk F, Urbaniak M, Swiniarski J, Kubiak T. Influence of boundary conditions on the behaviour of composite channel section subjected to pure bending – Experimental study. *Composite Structures* 2022; 279: 114727. https://doi.org/10.1016/j.compstruct.2021.114727.
17. Banat D, Mania RJ, Degenhardt R. Stress state failure analysis of thin-walled GLARE composite members subjected to axial loading in the post-buckling range. *Composite Structures* 2022; 289: 115468. https://doi.org/10.1016/j.compstruct.2022.115468.
18. Banat D, Mania RJ. Damage analysis of thin-walled GLARE members under axial compression – Numerical and experiment investigations. *Composite Structures* 2020; 241: 112102. https://doi.org/10.1016/j.compstruct.2020.112102.
19. Li W, Cai H, Li C, Wang K, Fang L. Progressive failure of laminated composites with a hole under compressive loading based on micro-mechanics. *Advanced Composite Materials* 2014; 23: 477-490. https://doi.org/10.1080/09243046.2014.915105.
20. Hu H, Niu F, Dou T, Zhang H. Rehabilitation Effect Evaluation of CFRP-Lined Prestressed Concrete Cylinder Pipe under Combined Loads Using Numerical Simulation. *Mathematical Problems in Engineering* 2018; 2018: 3268962. https://doi.org/10.1155/2018/3268962.
21. Samborski S, Rzeczkowski J, Korzec-Strzałka I. Experimental study of delamination process in elastically coupled laminates with the acoustic emission technique. *Engineering Structures* 2024; 300: 117196. https://doi.org/10.1016/j.engstruct.2023.117196.
22. Sabik A, Rucka M, Andrzejewska A, Wojtczak E. Tensile failure study of 3D printed PLA using DIC technique and FEM analysis. *Mechanics of Materials* 2022; 175: 104506. https://doi.org/10.1016/j.mechmat.2022.104506.
23. Rozylo P. Failure analysis of beam composite elements subjected to three-point bending using advanced numerical damage models. *Acta Mechanica et Automatica* 2023; 17: 133-144. https://doi.org/10.2478/ama-2023-0015.
24. Rozylo P. Study of the behavior of thin-walled composite structures with closed sections under three-point bending tests. *Advances in Science and Technology Research Journal* 2025; 19(6): 403-413. https://doi.org/10.12913/22998624/203459.
25. Gliszczynski A, Czechowski L. Collapse of channel section composite profile subjected to bending, Part I: Numerical investigations. *Composite Structures* 2017; 178: 383-394. https://doi.org/10.1016/j.compstruct.2017.07.033.
26. Jakubczak P, Gliszczynski A. Bienias J, Majerski K. Kubiak T. Collapse of channel section composite profile subjected to bending Part II: Failure analysis. *Composite Structures* 2017; 179: 1-20. https://doi.org/10.1016/j.compstruct.2017.07.052.
27. Heidari-Rarani M, Sayedain M. Finite element modeling strategies for 2D and 3D delamination propagation in composite DCB specimens using VCCT, CZM and XFEM approaches. *Theoretical and Applied Fracture Mechanics* 2019; 103: 102246. https:/doi.org/10.1016/j.tafmec.2019.102246.
28. Camanho PP, Davila CG, de Moura MF. Numerical simulation of mixed-mode progressive delamination in the composite materials, *Journal of Composite Materials* 2003; 37(16): 1415-1438. https://doi.org/10.1177/0021998303034505.
29. Ribeiro ML, Vandepitte D, Tita V. Damage model and progressive failure analyses for filament wound composite laminates. *Applied Composite Materials* 2013; 20: 975-992. https://doi.org/10.1007/s10443-013-9315-x.
30. Rozylo P, Debski H. Stability and load carrying capacity of thin-walled composite columns with square cross-section under axial compression. *Composite Structures* 2024; 329: 117795. https://doi.org/10.1016/j.compstruct.2023.117795.
31. Rozylo P. Limit states of thin-walled composite structures with closed sections under axial compression. *Composites Part B Engineering* 2024; 287: 111813. https://doi.org/10.1016/j.compositesb.2024.111813.

32. Rozylo P, Rogala M, Pasnik J. Buckling analysis of thin-walled composite structures with rectangular cross-sections under compressive load. *Materials* 2023; 16: 6835. https://doi.org/10.3390/ma16216835.
33. Rozylo P, Rogala M, Pasnik J. Load-Carrying Capacity of Thin-Walled Composite Columns with Rectangular Cross-Section under Axial Compression. *Materials* 2024; 17: 1615. https://doi.org/10.3390/ma17071615.
34. Wysmulski P, Debski H, Falkowicz K. Stability analysis of laminate profiles under eccentric load. *Composite Structures* 2020; 238: 111944. https://doi.org/10.1016/j.compstruct.2020.111944.
35. Falkowicz K. Experimental and numerical analysis of compression thin-walled composite plates weakened by cut-outs. *Archives of Civil Engineering* 2017, LXIII, 161-172. https://doi.org/10.1515/ace-2017-0047.
36. Falkowicz K, Wysmulski P, Debski H. Buckling Analysis of Laminated Plates with Asymmetric Layup by Approximation Method. *Materials* 2023; 16: 4948. https://doi.org/10.3390/ma16144948.
37. Rozylo P, Smagowski W, Pasnik J. Experimental Research in the Aspect of Determining the Mechanical and Strength Properties of the Composite Material Made of Carbon-Epoxy Composite. *Advances in Science and Technology Research Journal* 2023; 17(2): 232-246. https://doi.org/10.12913/22998624/161598.
38. Hodgkinson J.M. Mechanical Testing of Advanced Fibre Composites. Woodhead Publishing Ltd., Cambridge, 2000. https://doi.org/10.1201/9781439822791.
39. Ramkumar, R.; Rajaram, K.; Saravanan, P.; Venkatesh, R.; Saranya, K.; Jenaris, D.S. Determination of mechanical properties of CFRP composite reinforced with Abaca and Kenaf fibres. *Materials Today: Proceedings* 2022; 62: 5311-5316. https://doi.org/10.1016/j.matpr.2022.03.382.